

# Measurement methods of radial flow in relativistic heavy-ion collisions

Peng Yang,<sup>1</sup> Lin Li,<sup>2</sup> Yu Zhou,<sup>3</sup> Zhiming Li,<sup>1</sup> Mingmei Xu,<sup>1</sup> Yeyin Zhao,<sup>1</sup> and Yuanfang Wu<sup>1,\*</sup>

<sup>1</sup>*Key Laboratory of Quark and Lepton Physics (MOE) and Institute of Particle Physics,  
Central China Normal University, Wuhan 430079, China*

<sup>2</sup>*School of Science, Wuhan University of Technology, Wuhan 430070, China*

<sup>3</sup>*Department of Mathematics, University of California, Los Angeles, CA 90095, USA*

Radial flow can be directly extracted from the azimuthal distribution of mean transverse rapidity. We apply the event-plane method and the two-particle correlation method to estimate the anisotropic Fourier coefficient of the azimuthal distribution of mean transverse rapidity. Using the event sample generated by the AMPT model with string melting, we show that both methods are effective. For the two-particle correlation method to be reliable, the mean number of particles in an azimuthal bin must be above a certain threshold. Using these two methods, anisotropic radial flow can be estimated in a model-independent way in relativistic heavy-ion collisions.

PACS numbers: 25.75.Nq, 25.75.Dw, 25.75.Ld

## I. INTRODUCTION

Collectivity, or flow, is one of the main characteristics of the newly formed quark-gluon plasma (QGP) in relativistic heavy-ion collisions [1–4]. Traditionally, we have observed radial flow, direct flow, elliptic flow, triangular flow and so on. Radial flow and elliptic flow are the two prominent classes among them.

Elliptic flow is defined as the second Fourier component of the azimuthal multiplicity distribution. It is generated by the initial geometric asymmetry of non-central collisions, where the overlap of two incident nuclei is of an almond shape in the transverse coordinate plane. The minor axis of the overlap is in the reaction plane, which is spanned by the vector of impact parameter and beam direction [1, 4, 5]. This initial geometric asymmetry leads to a larger density gradient along the in-plane direction, i.e., the anisotropic distribution of final-state particles in momentum space. Therefore, elliptic flow provides information about initial conditions and system properties [2, 6].

Radial flow is originally deduced from an analysis of transverse momentum spectra in central collisions [1, 4, 7]. Later, it is generalized into two parameters: isotropic radial velocity and anisotropic radial velocity [8–12]. The isotropic radial velocity features the isotropic transverse expansion of the source at kinetic freeze-out. The anisotropic radial velocity presents the difference of the radial flow between the in-plane direction and the out-of-plane direction, and also arises in non-central collisions.

The interplay of radial expansion and elliptic flow results in what we observe as the particle mass splitting of the differential elliptic flow [3, 4, 6]. Namely, the heavier particles show smaller elliptic flow values. This mass ordering of elliptic flow has been well understood by hydro-

dynamics with a set of kinetic freeze-out constraints, i.e., radial flow, temperature, and source deformation [13, 14].

In addition, momentum transfer due to viscosity is proportional to the first derivative of the velocity in hydrodynamics [15, 16]. Bulk viscosity is associated with isotropic transverse velocity, while shear viscosity is associated with the anisotropic transverse velocity. The proportion constants are equal to the bulk and shear viscosities respectively. Therefore, the determination of anisotropic radial flow is essential for hydrodynamic calculations and for measuring the shear viscosity in relativistic heavy-ion collisions [17–19].

Conventionally, anisotropic radial flow is extracted by fitting the transverse momentum spectrum of particles with the Blast-Wave parameterization [20, 21]. To minimize the  $\chi^2$  of the fitting, the spectra of all particle species are fitted simultaneously. For the relativistic heavy-ion collisions at AGS, RHIC and LHC energies, the fitting results have all been presented [22–25]. However, these results are obviously model-dependent. Therefore, a model-independent measurement is called for.

In order to measure radial flow, we had introduced the mean-transverse-rapidity (MTR) and its azimuthal distribution, replacing velocity with rapidity in the original definition of radial flow [12, 15, 26]. The MTR is averaged over the number of particles in an azimuthal angle bin. It presents the raw kinetic expansion in a specified azimuthal direction.

The azimuthal distribution of the MTR presents the transverse expansion of the source at kinetic freeze-out [15, 27, 28]. The second Fourier coefficient of this distribution features the anisotropic kinetic expansion, and is consistent with the anisotropic radial flow extracted from the Blast-Wave parameterization [12].

The aim of this paper is to estimate the anisotropic radial flow in relativistic heavy-ion collisions. This estimation is similar to how we estimate elliptic flow, where the reaction plane cannot be measured directly due to random fluctuations of the impact parameter vector, and is instead estimated from the reconstructed particles. This estimation method is the so-called event-plane method

\*Electronic address:  
lilin'phy@whut.edu.cn,  
xumm@mail.ccnu.edu.cn

wuyf@mail.ccnu.edu.cn,  
lizm@mail.ccnu.edu.cn,

(EPM) [29–31]. Later, it is found that the two-particle correlation method (TPCM) can also be used in place of the EPM to estimate the elliptic flow [32–36].

In this paper, we first describe the EPM and the TPCM that are designed to estimate the anisotropic coefficients of azimuthal distributions for both total-transverse-rapidity (TTR) and MTR in Section II. Then, we demonstrate the effectivity of both methods using the event sample generated by the AMPT model with string melting in Section III. The limitation of the TPCM is discussed in Section IV. Finally, summary and conclusions are presented in section V.

## II. MEASUREMENT METHODS

Transverse rapidity is defined as [2, 12, 15, 26],

$$y_T = \ln\left(\frac{m_T + p_T}{m_0}\right), \quad (1)$$

where  $m_0$  is the particle mass in the rest frame,  $p_T$  is transverse momentum, and  $m_T = \sqrt{m_0^2 + p_T^2}$  is transverse mass.

The total-transverse-rapidity (TTR) of the  $m$ th azimuthal bin is the summation of all particles' transverse rapidities in an event, and its average is [12, 15, 26],

$$\langle Y_T(\phi_m - \Psi_r) \rangle = \frac{1}{N_{\text{event}}} \sum_{k=1}^{N_{\text{event}}} \sum_{i=1}^{N_m^k} y_{T,i}^k(\phi_m - \Psi_r). \quad (2)$$

It measures total transverse expansion in a specified azimuthal bin  $(\phi_m - \Psi_r)$ , where  $\Psi_r$  is the reaction plane angle.  $\phi_m$  is the  $m$ th azimuthal angle bin. The bin width is  $2\pi/N_{\text{bin}}$ .  $N_{\text{bin}}$  is the total number of bins.  $y_{T,i}^k(\phi_m - \Psi_r)$  is the transverse rapidity of  $i$ th particle in  $k$ th event and  $m$ th azimuthal angle bin.  $N_m^k$  is the total number of particles in the  $k$ th event and the  $m$ th azimuthal angle bin.  $N_{\text{event}}$  is the total number of events.

The mean-transverse-rapidity (MTR) of the  $m$ th azimuthal bin is defined as,

$$\langle\langle y_T(\phi_m - \Psi_r) \rangle\rangle = \frac{1}{N_{\text{event}}} \sum_{k=1}^{N_{\text{event}}} \frac{1}{N_m^k} \sum_{i=1}^{N_m^k} y_{T,i}^k(\phi_m - \Psi_r), \quad (3)$$

where  $\langle\langle \dots \rangle\rangle$  is first averaged over the number of particles in the  $k$ th event and the  $m$ th azimuthal angle bin  $N_m^k$ , and then over the total number of events. It measures the raw kinetic expansion in a specified azimuthal direction. The contribution of the number of particles is removed by the first average.

The Fourier expansions of azimuthal TTR and MTR distributions are,

$$\frac{d\langle Y_T(\phi - \Psi_r) \rangle}{d(\phi - \Psi_r)} = v_0(Y_T) \left( 1 + \sum_{n=1}^{\infty} 2v_n(Y_T) \cos[n(\phi - \Psi_r)] \right), \quad (4)$$

and

$$\frac{d\langle\langle y_T(\phi - \Psi_r) \rangle\rangle}{d(\phi - \Psi_r)} = v_0(y_T) \left( 1 + \sum_{n=1}^{\infty} 2v_n(y_T) \cos[n(\phi - \Psi_r)] \right), \quad (5)$$

where azimuthal-angle-independent  $v_0(Y_T)$  and  $v_0(y_T)$  are isotropic TTR flow and radial flow respectively. The second Fourier coefficients  $v_2(Y_T)$  and  $v_2(y_T)$  are defined as anisotropic TTR flow and radial flow respectively [12, 15, 26].

They are similar to the mean multiplicity in the  $m$ th azimuthal angle bin, i.e.,

$$\langle N(\phi_m - \Psi_r) \rangle = \frac{1}{N_{\text{event}}} \sum_{k=1}^{N_{\text{event}}} N^k(\phi_m - \Psi_r), \quad (6)$$

where  $N^k(\phi_m - \Psi_r)$  is the number of particles in  $k$ th event and  $(\phi_m - \Psi_r)$  direction. Its azimuthal distribution in Fourier expansion is,

$$\frac{d\langle N(\phi - \Psi_r) \rangle}{d(\phi - \Psi_r)} = v_0(N) \left( 1 + \sum_{n=1}^{\infty} 2v_n(N) \cos[n(\phi - \Psi_r)] \right), \quad (7)$$

where  $v_0(N)$  is azimuthal-angle-independent.  $v_2(N)$  is elliptic flow, which is estimated in practice by the EPM and the TPCM. In the following, we apply these two methods to estimate  $v_2(Y_T)$  and  $v_2(y_T)$ .

### A. The event-plane method

In nuclear-nuclear collisions, the azimuthal angle of the final state particle is measured with respect to the reaction plane. However, the angle of reaction plane is unknown in experiments and fluctuates from event to event. Usually, a reconstructed event-plane is considered as a substitute [29], i.e.,  $\Psi_n$  of the  $n$ th coefficient is given by,

$$\Psi_n = \left( \tan^{-1} \frac{Q_{n,y}}{Q_{n,x}} \right) / n, \quad (8)$$

where  $Q_n$  is flow vector and defined as,

$$Q_{n,x} = \sum_{i=1}^M \omega_i \cos(n\phi_i) = Q_n \cos(n\Psi_n), \quad (9)$$

$$Q_{n,y} = \sum_{i=1}^M \omega_i \sin(n\phi_i) = Q_n \sin(n\Psi_n). \quad (10)$$

$M$  is the number of particles used in the event-plane determination.  $\phi_i$  and  $\omega_i$  are the azimuthal angle and the weight of  $i$ th particle.

A general Fourier expansion with respect to the event-plane ( $\Psi_n$ ) can be expressed as,

$$\frac{d\langle \omega N(\phi - \Psi_n) \rangle}{d(\phi - \Psi_n)} = v_0(\omega N) \left( 1 + \sum_{n=1}^{\infty} 2v_n^{\text{obs}}(\omega N) \cos[n(\phi - \Psi_n)] \right), \quad (11)$$

where weight  $\omega$  changes with the observable [29], such as different kinds of flow defined in Eqs. (4), (5) and (7).

For multiplicity, the weight is unity, and Eq. (11) corresponds to Eq. (7). Its  $v_2^{\text{obs}}(N)$  is,

$$v_2^{\text{obs}}(N) = \frac{1}{N_{\text{event}}} \sum_{k=1}^{N_{\text{event}}} \left( \frac{1}{N^k} \sum_{i=1}^{N^k} \cos[2(\phi_i^k - \Psi_2)] \right), \quad (12)$$

where  $\Psi_2$  is the event-plane angle of the second harmonic, and  $N^k$  is the total number of particles in  $k$ th event.

For the TTR and MTR, their weights are  $\omega_i = y_{T,i}$  and  $\omega_i = y_{T,i,m}/N_m$ , respectively. Their  $v_2^{\text{obs}}(Y_T)$  and  $v_2^{\text{obs}}(y_T)$  are,

$$v_2^{\text{obs}}(Y_T) = \frac{1}{N_{\text{event}}} \sum_{k=1}^{N_{\text{event}}} \left( \frac{1}{\sum_{i=1}^{N^k} y_{T,i}^k} \sum_{i=1}^{N^k} y_{T,i}^k \cos[2(\phi_i^k - \Psi_2)] \right), \quad (13)$$

and

$$v_2^{\text{obs}}(y_T) = \frac{1}{N_{\text{event}}} \sum_{k=1}^{N_{\text{event}}} \left( \frac{1}{\sum_{m=1}^{N_{\text{bin}}} \frac{1}{N_m^k} \sum_{k=1}^{N_m^k} y_{T,i,m}^k} \sum_{m=1}^{N_{\text{bin}}} \frac{1}{N_m^k} \sum_{k=1}^{N_m^k} y_{T,i,m}^k \cos[2(\phi_{i,m}^k - \Psi_2)] \right). \quad (14)$$

With finite multiplicity,  $v_2^{\text{obs}}(N)$  has to be corrected for the event-plane resolution [4, 29], i.e.,

$$\mathfrak{R}_2 = \langle \cos[2(\Psi_2 - \Psi_r)] \rangle, \quad (15)$$

which is obtained by the iteration of sub-event-plane resolution. The sub-event is usually constructed in a longitudinal rapidity window that is different from the particles of interest [23, 37]. Therefore, the elliptic flow is,

$$v_2(N) = v_2^{\text{obs}}(N)/\mathfrak{R}_2. \quad (16)$$

After the same corrections for  $v_2^{\text{obs}}(Y_T)$  and  $v_2^{\text{obs}}(y_T)$ ,  $v_2(Y_T)$  and  $v_2(y_T)$  are,

$$v_2(Y_T) = v_2^{\text{obs}}(Y_T)/\mathfrak{R}_2, \quad (17)$$

and

$$v_2(y_T) = v_2^{\text{obs}}(y_T)/\mathfrak{R}_2. \quad (18)$$

## B. The two-particle correlation method

The coefficients of Fourier expansion Eq. (7) can also be estimated by the TPCM [30], i.e.,

$$\langle \cos[n(\phi_1 - \phi_2)] \rangle = \langle e^{in(\phi_1 - \phi_2)} \rangle = \langle v_n^2 \rangle + \delta_n. \quad (19)$$

Here a cross-term that depends both on  $v_n$  and  $\delta_n$  is neglected, as it is very small in most cases of interest.  $\delta_2$  represents the so-called non-flow contribution and is irrelevant to initial geometry. All correlations are first averaged over all particle pairs in a given event, and then over all events. The latter average involves weight depending on event. For convenience, single-event average two-particle azimuthal correlations is defined as,

$$\langle 2 \rangle^k \equiv \frac{1}{\sum_{i,j=1,i \neq j}^{N^k} \omega_i^k \omega_j^k} \sum_{i,j=1,i \neq j}^{N^k} \omega_i^k \omega_j^k e^{in(\phi_i^k - \phi_j^k)}. \quad (20)$$

Its average over all events is,

$$\begin{aligned} \langle \langle 2 \rangle \rangle &\equiv \frac{\sum_{k=1}^{N_{\text{event}}} \sum_{i,j=1,i \neq j}^{N^k} \omega_i^k \omega_j^k \langle 2 \rangle^k}{\sum_{k=1}^{N_{\text{event}}} \sum_{i,j=1,i \neq j}^{N^k} \omega_i^k \omega_j^k} \\ &= \frac{\sum_{k=1}^{N_{\text{event}}} \sum_{i,j=1,i \neq j}^{N^k} \omega_i^k \omega_j^k e^{in(\phi_i^k - \phi_j^k)}}{\sum_{k=1}^{N_{\text{event}}} \sum_{i,j=1,i \neq j}^{N^k} \omega_i^k \omega_j^k}. \end{aligned} \quad (21)$$

For multiplicity and TTR, their weights are  $\omega_i = 1$  and  $\omega_i = y_{T,i}$ , respectively. So their  $\langle \langle 2 \rangle \rangle$  are

$$\langle\langle 2 \rangle\rangle_N = \frac{\sum_{k=1}^{N_{\text{event}}} \sum_{i,j,i \neq j}^{N^k} e^{in(\phi_i^k - \phi_j^k)}}{\sum_{k=1}^{N_{\text{event}}} N^k (N^k - 1)}, \quad (22)$$

and

$$\langle\langle 2 \rangle\rangle_{Y_T} = \frac{\sum_{k=1}^{N_{\text{event}}} \sum_{i,j,i \neq j}^{N^k} y_{T,i}^k y_{T,j}^k e^{in(\phi_i^k - \phi_j^k)}}{\sum_{k=1}^{N_{\text{event}}} \sum_{i,j,i \neq j}^{N^k} y_{T,i}^k y_{T,j}^k}. \quad (23)$$

Elliptic flow can be estimated from two-particle correlations by [30, 31],

$$v_2(N) = \sqrt{\langle\langle 2 \rangle\rangle_N}. \quad (24)$$

Similarly, corresponding anisotropic coefficient of TTR can be estimated by,

$$v_2(Y_T) = \sqrt{\langle\langle 2 \rangle\rangle_{Y_T}}. \quad (25)$$

Eq. (25) is obtained in the same way as Eq. (24), except for the non-unit weight factor.

For MTR, its weight is  $\omega_i = y_{T,i,m}/N_m$ . The two correlated particles could come from the same azimuthal angle bin or from different bins. If they come from different bins, the single-event average two-particle azimuthal correlations is:

$$\langle 2 \rangle_{\text{d}}^k = \sum_{m,n=1, m \neq n}^{N_{\text{bin}}} \left( \frac{1}{N_m^k N_n^k} \sum_{i=1}^{N_m^k} \sum_{j=1}^{N_n^k} y_{T,i,m}^k y_{T,j,n}^k e^{in(\phi_{i,m}^k - \phi_{j,n}^k)} \right). \quad (26)$$

Here  $N_m^k$  and  $N_n^k$  are the numbers of particles in  $m$ th and  $n$ th bin, respectively. If they come from the same bin, the single-event average two-particle azimuthal correlations is,

$$\langle 2 \rangle_{\text{s}}^k = \sum_{m=1}^{N_{\text{bin}}} \left( \frac{1}{N_m^k (N_m^k - 1)} \sum_{i,j=1, i \neq j}^{N_m^k} y_{T,i,m}^k y_{T,j,m}^k e^{in(\phi_{i,m}^k - \phi_{j,m}^k)} \right). \quad (27)$$

Therefore,  $\langle\langle 2 \rangle\rangle$  of the azimuthal distribution of MTR is,

$$\langle\langle 2 \rangle\rangle_{Y_T} = \frac{\sum_{k=1}^{N_{\text{event}}} \langle 2 \rangle_{\text{d}}^k + \langle 2 \rangle_{\text{s}}^k}{\sum_{k=1}^{N_{\text{event}}} W^k}, \quad (28)$$

where  $W^k$  is the event weight, i.e.,

$$W^k = \sum_{m,n=1, m \neq n}^{N_{\text{bin}}} \frac{1}{N_m^k N_n^k} \sum_{i=1}^{N_m^k} \sum_{j=1}^{N_n^k} y_{T,i,m}^k y_{T,j,n}^k + \sum_{m=1}^{N_{\text{bin}}} \frac{1}{N_m^k (N_m^k - 1)} \sum_{i,j=1, i \neq j}^{N_m^k} y_{T,i,m}^k y_{T,j,m}^k. \quad (29)$$

The corresponding anisotropic radial flow is,

$$v_2(y_T) = \sqrt{\langle\langle 2 \rangle\rangle_{Y_T}}. \quad (30)$$

Up to now, we derive the anisotropic coefficients of azimuthal multiplicity, TTR and MTR distributions by both the EPM and the TPCM. In order to check how these two methods work in practice, we apply them to the event sample generated by Monte Carlo simulation in the following section.

### III. APPLICATION

The AMPT model with string melting [38, 39] can reproduce the observed elliptic flow at RHIC [32–35]. The event sample generated by this model has the basic characteristics of flows in general, and can be used to test the effectivity of the two aforementioned methods.

With this model, we generate four million events for Au+Au collisions at 200 GeV. The analysis is presented in the kinetic ranges  $|\eta| \leq 2.5$ , and  $p_T \in [0.15, 2]$  GeV/c which is the same as RHIC/STAR [33, 35]. Nine centrality bins are defined by the  $N_{\text{part}}$  corresponding to the nine multiplicity-ranges, consistent with those at RHIC/STAR [35].

For the event-plane method (EPM), two sub-events ((a) and (b)) for resolution corrections are constructed in two longitudinal symmetry windows  $|\eta| \in [3.3, 4.5]$ , similar to those at RHIC/STAR [23]. We also use a random method to make the number of charged particles in each sub-event even [29, 33].

Since the azimuthal angle of the true reaction plane  $\Psi_r$  is known and set to zero in this model,  $v_2(Y_T)$ ,  $v_2(N)$ , and  $v_2(y_T)$  can be directly obtained by the corresponding azimuthal distributions. These directly obtained  $v_2(Y_T)$ ,  $v_2(N)$ , and  $v_2(y_T)$  can be regarded as their true values. Their centrality dependence are represented in Fig. 1(a) by solid blue triangles, black dots and red stars, respectively.

In Fig. 1(a), three kinds of flows have similar centrality dependence, consistent with those obtained from UrQMD [27, 28, 40]. In each of the centrality interval,  $v_2(Y_T)$  is the largest,  $v_2(N)$  is medial, and  $v_2(y_T)$  is the smallest. It is no surprise that  $v_2(N)$  and  $v_2(y_T)$  are both smaller than  $v_2(Y_T)$ . From the definitions of Eqs. (2), (3), and (6), total-transverse-rapidity (TTR)

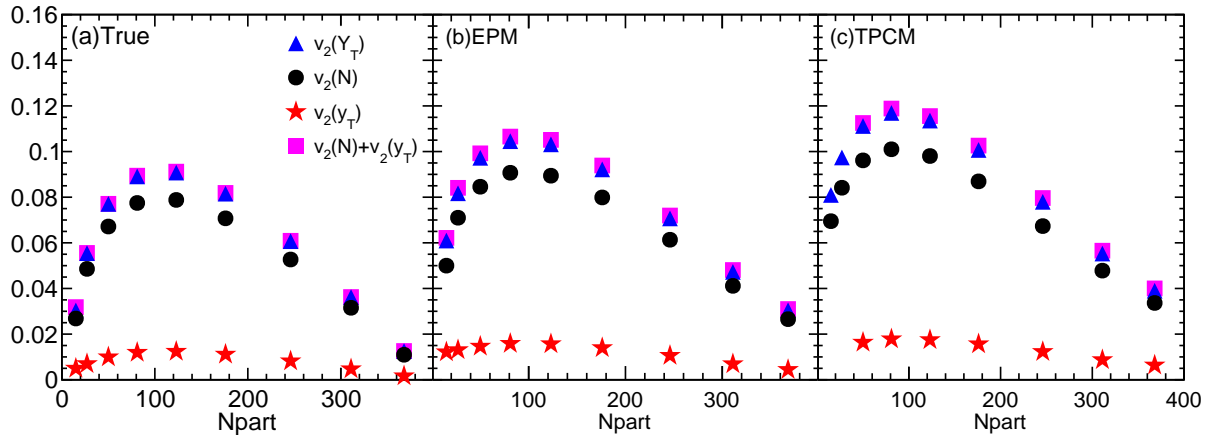


FIG. 1: Centrality dependence of elliptic flow (solid black dots), anisotropic radial flow (solid red stars), anisotropic TTR flow (solid blue triangles), and the summation of elliptic flow and anisotropic radial flow (solid purple squares). (a) is the true results. (b) and (c) are the results estimated by the EPM and the TPCM, respectively. The error of each point is smaller than the symbol size.

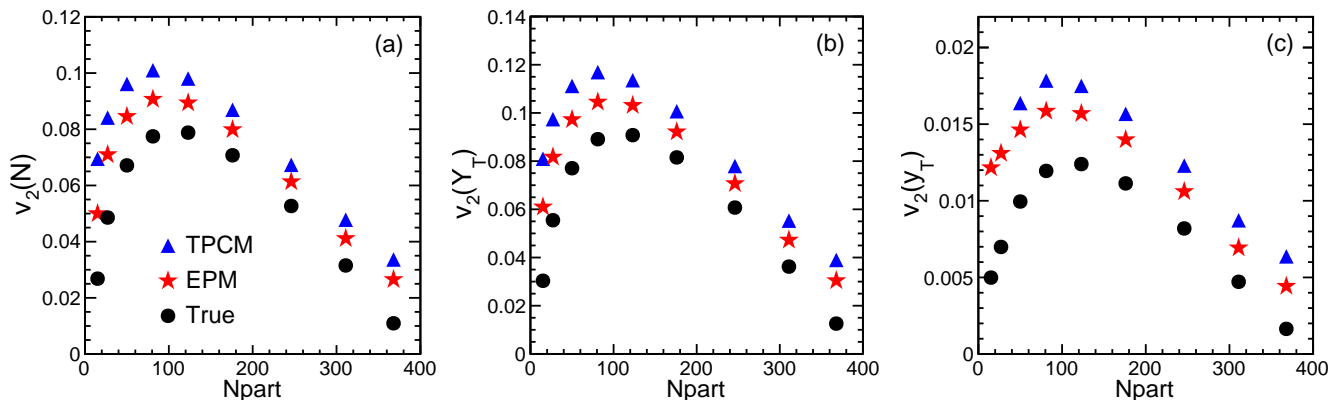


FIG. 2: Centrality dependence of  $v_2(N)$  (a),  $v_2(Y_T)$  (b), and  $v_2(y_T)$  (c), where solid black dots are true values, solid red stars and solid blue triangles are estimated by the EPM and the TPCM, respectively. The error of each point is smaller than the symbol size.

contains the contributions from both the number of particles (multiplicity), and the transverse movement. Mean-transverse-rapidity (MTR) is raw kinetics, and the influence of multiplicity is excluded. Therefore,  $v_2(y_T)$  and  $v_2(N)$  are both smaller than  $v_2(Y_T)$ .

It is interesting that  $v_2(y_T) + v_2(N)$  (purple squares) overlaps with  $v_2(Y_T)$  (blue triangles) at each of the nine centralities. This relationship shows that the anisotropic radial flow and elliptic flow are additive, although MTR and multiplicity are not simply related to TTR.

In order to compare the anisotropic coefficients estimated by the two methods with their true values,  $v_2(N)$ ,  $v_2(Y_T)$  and  $v_2(y_T)$  are presented in Fig. 2(a), (b) and (c), respectively, where solid black dots are the true values,

solid red stars and blue triangles are estimated by the event-plane method (EPM) and the two-particle correlation method (TPCM).

For  $v_2(N)$  as shown in Fig. 2(a), in each centrality interval, the black dot is the lowest, the red star is in the middle and the blue triangle is the highest. This shows that the estimation given by TPCM is higher than the estimation given by EPM, and the estimations given these two methods are both higher than the true value. The excess parts are the contributions of non-flow and flow fluctuations [41, 42]. Nevertheless, the difference is roughly an overall shift. The general trends of three data sets are consistent with each other, and with the expectation that the larger elliptic flow appears in the mid-central colli-

sions, and small elliptic flow in peripheral and central collisions. Therefore, both methods can be considered as a valid estimation of true elliptic flow.

Similarly, for  $v_2(Y_T)$  as shown in Fig. 2(b), in each centrality interval, three kinds of points have the same position ordering as shown in Fig. 2(a), i.e., the lowest black dot, the middle red star and the highest blue triangle. By the same reasoning, these results demonstrate that the both methods are effective in estimating  $v_2(Y_T)$ .

For  $v_2(y_T)$  as shown in Fig. 2(c), three kinds of points also display the same ordering as shown in Fig. 2(a) and 2(b), i.e., the lowest black dots, the middle red stars and the highest blue triangles for the seven middle and central collisions. These results are not really surprising. As even in some Toy Monte Carlo studies, where there is only flow fluctuations and no systematic biases due to nonflow, the elliptic flow given by the EPM and the TPCM are still different [42].

The centrality dependence of elliptic flow, anisotropic TTR flow and radial flow estimated by the EPM and the TPCM are presented in Fig. 1(b) and 1(c) respectively, in comparison to their true values in Fig. 1(a). The summations of elliptic flow  $v_2(N)$  and anisotropic radial flow  $v_2(y_T)$  (purple squares) estimated by these two methods also overlap with corresponding anisotropic TTR flow  $v_2(Y_T)$  (blue triangles), consistent with the case in Fig. 1(a). Therefore, the elliptic flow and anisotropic radial flow estimated by these two methods are also additive, just like their true values. This demonstrates that the two methods are equally effective.

However, the two-particle-correlation method (TPCM) is ineffective in estimating  $v_2(y_T)$  for the two peripheral-collision bins. We will show in the following section why and how the TPCM fails.

#### IV. THE LIMITATION OF THE TPCM

$v_2(y_T)$  given by the TPCM in Eq. (30) is the square root of  $\langle\langle 2 \rangle\rangle_{y_T}$ . For the two peripheral-collision bins,  $\langle\langle 2 \rangle\rangle_{y_T}$  becomes negative. This is why the TPCM fails.

We can understand the cause of this problem from the original definition of mean-transverse-rapidity (MTR). MTR is defined to be averaged over  $N_m$  (the number of particles in the  $m$ th bin). If all particles are uniformly distributed in the whole azimuthal region,  $N_m \sim N/N_{\text{bin}}$  ( $N$  is multiplicity, and  $N_{\text{bin}}$  is the total number of bins). Now, assuming  $\langle\langle 2 \rangle\rangle_{y_T}$  is well-defined, we should have selected a proper  $N_{\text{bin}}$ , for which  $N_m$  is large enough.

To examine the proper range of  $N_{\text{bin}}$ ,  $\langle\langle 2 \rangle\rangle_{y_T}$  versus  $N_{\text{bin}}$  at the nine centralities are presented in Fig. 3. For mid-central collisions and central collisions,  $\langle\langle 2 \rangle\rangle_{y_T}$  decreases with  $N_{\text{bin}}$  when  $N_{\text{bin}} \leq 20$ , and then becomes independent of  $N_{\text{bin}}$  when  $N_{\text{bin}} \geq 20$ . There is a wide range of  $N_{\text{bin}}$ , where  $\langle\langle 2 \rangle\rangle_{y_T}$  stays flat. This range guarantees that  $\langle\langle 2 \rangle\rangle_{y_T}$  is independent of  $N_{\text{bin}}$ . Therefore, we choose  $N_{\text{bin}} = 25$  for all the aforementioned analysis.

However, for the two peripheral-collision bins,  $\langle\langle 2 \rangle\rangle_{y_T}$

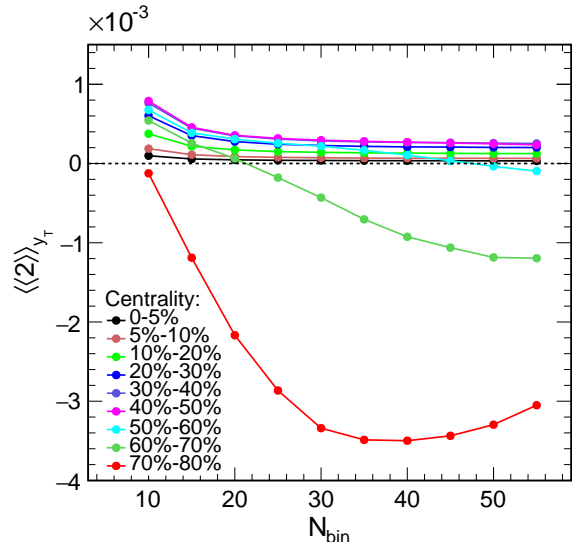


FIG. 3:  $\langle\langle 2 \rangle\rangle_{y_T}$  versus  $N_{\text{bin}}$  at the nine centralities, where the error of each point is smaller than the symbol size.

rapidly decreases to negative as  $N_{\text{bin}}$  increases. Obviously, this is not caused by change in  $N_{\text{bin}}$ , but instead by the decrease of multiplicity  $N$  from central to peripheral collisions. When  $N_{\text{bin}}$  is fixed,  $N_m$  is solely proportional to  $N$ . Therefore,  $N_m$  also decreases from central to peripheral collisions.

To find the lower threshold of  $\langle N_m \rangle$  in general, we randomly drop some particles in each event. Using this method, we can show how  $\langle\langle 2 \rangle\rangle_{y_T}$  changes with  $\langle N_m \rangle$ , and where in each centrality interval the TPCM becomes invalid.

$\langle\langle 2 \rangle\rangle_{y_T}$  versus  $\langle N_m \rangle$  for four cases are presented in Fig. 4(a), (b), (c) and (d). For the two upper subfigures, we choose the pseudorapidity range  $|\eta| \leq 2.5$ , and  $N_{\text{bin}} = 25$  for Fig. 4(a) and  $N_{\text{bin}} = 35$  for Fig. 4(b). In Fig. 4(a), with decrease of  $\langle N_m \rangle$ ,  $\langle\langle 2 \rangle\rangle_{y_T}$  stays flat and positive. This implies that  $\langle\langle 2 \rangle\rangle_{y_T}$  can still be estimated correctly even though some particles in each of the events are dropped. When  $\langle N_m \rangle$  decreases even lower,  $\langle\langle 2 \rangle\rangle_{y_T}$  rapidly drops to negative. This implies that the correlations between the two particles decrease significantly, and the method becomes invalid. Meanwhile, Fig. 4(b) also shows the same  $\langle N_m \rangle$  which makes  $\langle\langle 2 \rangle\rangle_{y_T}$  rapidly drop to negative. Therefore, independent of  $N_{\text{bin}}$ , as long as the mean number of particles in a bin is less than 10, the TPCM will fail.

For the two lower subfigures, we choose the pseudorapidity range  $|\eta| \leq 1$ , and  $N_{\text{bin}} = 25$  for Fig. 4(c) and  $N_{\text{bin}} = 35$  for Fig. 4(d). In contrast with the two upper row subfigures, narrow pseudorapidity range makes the total multiplicity smaller. The general trends in Fig. 4(c) and 4(d) are consistent with each other and with two upper subfigures. This means that  $\langle\langle 2 \rangle\rangle_{y_T}$  is independent

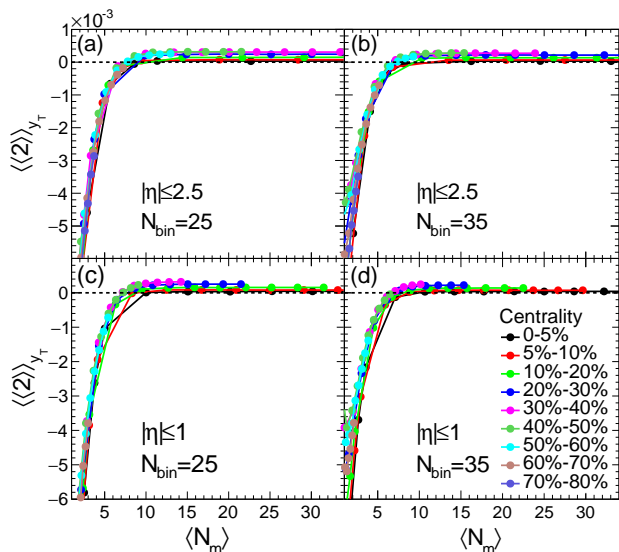


FIG. 4:  $\langle\langle 2 \rangle\rangle_{y_T}$  versus  $\langle N_m \rangle$  at the nine centralities, where the error of each point is smaller than the symbol size.

of the total mean multiplicity  $\langle N \rangle$  and  $N_{\text{bin}}$ , but is dependent on  $\langle N_m \rangle$ . Both Fig. 4(c) and 4(d) show negative  $\langle\langle 2 \rangle\rangle_{y_T}$  when  $\langle N_m \rangle < 10$ . Therefore, the lower threshold of  $\langle N_m \rangle$  is 10 for the TPCM.

In addition, one may ask why there is no such lower threshold in the EPM. This is because  $v_2(y_T)$  given by Eq. (30) is of higher order than that given by Eq. (18). The right side of Eq. (30) is the square root of two-particle correlations. Therefore, higher precision is required for the TPCM.

Moreover, as shown in Fig. 1, anisotropic radial flow is the smallest one among three. Its measurement is more difficult than anisotropic TTR flow, or elliptic flow. Therefore, a larger number of two-particle pairs is required.

## V. SUMMARY AND CONCLUSIONS

Anisotropic radial flow can be directly extracted from the azimuthal distribution of the mean-transverse-

rapidity (MTR). First, we apply the event-plane method (EPM) and the two-particle correlation method (TPCM) to estimate the anisotropic coefficients of the azimuthal distributions of total-transverse-rapidity (TTR) and MTR in relativistic heavy-ion collisions.

Then, using the event sample of Au+Au collisions at 200 GeV generated by the AMPT model with string melting, we show that the EPM and the TPCM are both effective in estimating the anisotropic TTR flow. The EPM is also effective in estimating anisotropic radial flow.

For central collisions and mid-central collisions, the TPCM is effective in estimating anisotropic radial flow. However, for the two peripheral-collision bins, this method fails when the mean number of particles in a bin becomes less than 10.

Therefore, anisotropic radial flow can be estimated in a model-independent way by the EPM and the TPCM in relativistic heavy-ion collisions. For the TPCM to be reliable, the mean number of particles in an azimuthal bin must be above a certain threshold.

We find that the summation of the true elliptic flow and true anisotropic radial flow is consistent with the true anisotropic TTR flow. This relationship also holds for the corresponding coefficients estimated by the EPM and the TPCM. Therefore, elliptic flow and anisotropic radial flow are additive.

## VI. ACKNOWLEDGEMENT

We are very grateful to Dr. Gang Wang for his valuable comments and suggestions. We thank Dr. Aihong Tang, Fuqiang Wang, You Zhou, and Ziwei Lin for helpful discussions. This work is supported in part by the Ministry of Science and Technology (MoST) under grant No. 2016YFE0104800 and the Fundamental Research Funds for the Central Universities under Grant No. CCNU19ZN019.

[1] J. Y. Ollitrault, Nucl. Phys. A, 638, 195c (1998).  
[2] P. Braun-Munzinger, J. Stachel, Nature 448, Issue 7151, 302-309 (2007).  
[3] S. A. Voloshin, Phys. Rev. C 55, 1630 (1997).  
[4] S. A. Voloshin, A. M. Poskanzer, and R. Snellings, arXiv: 0809.2949 (2008).  
[5] T. Hirano, arXiv: 9904082 (1999).  
[6] P. Danielewicz, Phys. Rev. C 51, 716 (1995).  
[7] C. M. Hung and E. Shuryak, Phys. Rev. C 57, 1891(1998).

[8] P. Huovinen and P. V. Ruuskanen, Ann. Rev. Nucl. Part. Sci. 56, 163 (2006).  
[9] M. Shao, L. Yi, Z. B. Tang, H. F. Chen et al., J. Phys. G 37, 085104 (2010).  
[10] Z. B. Tang, L. Yi, L. J. Ruan et al., Chin. Phys. Lett. 30(3), 031231 (2013).  
[11] J. Chen, J. Deng, Z. B. Tang et al., arXiv: 2012.02986 (2020).  
[12] L. Li, N. Li, and Y. F. Wu, J. Phys. G 40, 075104 (2013).  
[13] P. Huovinen, P. F. Kolb, U. W. Heinz, P. V. Ruuskanen,

- and S. A. Voloshin, Phys. Lett. B 503, 58 (2001).
- [14] N. Borghini and J. Y. Ollitrault, Phys. Lett. B 642, 227 (2006).
- [15] L. Li, N. Li, and Y. F. Wu, Chinese Physics C 36(5), 423-428 (2012).
- [16] L. D. Landau and E. M. Lifschitz, Fluid Mechanics. Institute of Physical Problems, U.S.S.R. Academy of Sciences, Volume 6, Course of Theoretical Physics.
- [17] C. Shen and U. Heinz, Phys. Rev. C 85, 054902 (2012).
- [18] Iu. A. Karpenko, P. Huovinen, H. Petersen, and M. Bleicher, Phys. Rev. C 91, 064901 (2015).
- [19] P. F. Liu and R. A. Lacey, Phys. Rev. C 98, 021902 (2018).
- [20] E. Schnedermann, J. Sollfrank, and U. W. Heinz, Phys. Rev. C 48, 2462 (1993).
- [21] Y. Oh, Z. W. Lin, and C. M. Ko, Phys. Rev. C 80, 064902 (2009).
- [22] J. Barrette et al. [E877 Collaboration], Phys. Rev. C 62, 024901 (2000).
- [23] L. Adamczyk et al. [STAR Collaboration], Phys. Rev. C 93, 014907 (2016).
- [24] L. Adamczyk et al. [STAR Collaboration], Phys. Rev. C 96, 044904 (2017).
- [25] B. Abelev et al. [ALICE Collaboration], Phys. Rev. C 88, 044910 (2013).
- [26] P. Yang, L. Li, and Y. F. Wu, Beijing: Sciencepaper Online, 201404-454 (2014).
- [27] S. Sarkar, P. Mali, and A. Mukhopadhyay, Phys. Rev. C 95, 014908 (2017).
- [28] S. Sarkar, P. Mali, S. Ghosh, and A. Mukhopadhyay, Advances in High Energy Physics 2018, 7453752 (2018).
- [29] A. M. Poskanzer and S. A. Voloshin, Phys. Rev. C 58, 1671 (1998).
- [30] A. Bilandzic, R. Snellings, and S. A. Voloshin, Phys. Rev. C 83, 044913 (2011).
- [31] N. Borghini, P. M. Dinh, and J. Y. Ollitrault, Phys. Rev. C 64, 054901 (2001).
- [32] C. Adler et al. [STAR Collaboration], Phys. Rev. C 66, 034904 (2002).
- [33] B. I. Abelev et al. [STAR Collaboration], Phys. Rev. C 77, 054901 (2008).
- [34] L. Adamczyk et al. [STAR Collaboration], Phys. Rev. C 86, 054908 (2012).
- [35] J. Adams et al. [STAR Collaboration], Phys. Rev. C 72, 014904 (2005).
- [36] S. Wang, Y. Z. Jiang, and Y. M. Liu, Phys. Rev. C 44, 1091 (1991).
- [37] J. Y. Ollitrault, Phys. Rev. D 48, 1132 (1993).
- [38] Z. W. Lin and C. M. Ko, Phys. Rev. C 65, 034904 (2002).
- [39] Z. W. Lin, C. M. Ko, B. A. Li, B. Zhang and S. Pal, Phys. Rev. C 72, 064901 (2005).
- [40] S. Sarkar and A. Mukhopadhyay, Nucl. Phys. 60 (2015).
- [41] J. Y. Ollitrault, A. M. Poskanzer and S. A. Voloshin, Phys. Rev. C 80, 014904 (2009).
- [42] M. Luzum and J. Y. Ollitrault, Phys. Rev. C 87, 044907 (2013).